



## Air Bubbles Displacement in Yield Stress Fluids

M. F. Naccache<sup>†</sup>, A. A. Abdu and C. Abreu

*Department of Mechanical Engineering, Pontifícia Universidade Católica-RJ Rua Marquês de São Vicente  
225, Rio de Janeiro, RJ 22453-900, Brazil*

<sup>†</sup>Corresponding Author Email: [naccache@puc-rio.br](mailto:naccache@puc-rio.br)

(Received March 13, 2019; accepted August 10, 2019)

### ABSTRACT

The motion of air bubbles in a yield stress fluid is analyzed numerically using a 2D approach and the finite volume technique. The multiphase flow is simulated using the volume of fluid method (VoF), which solves the conservation equations of mass and momentum coupled to a transport equation for the volume fraction of the fluids. The effects of yield stress, bubble size, number and position of bubbles rising in a viscoplastic fluid confined between vertical parallel plates are analyzed and discussed. The results indicate that the yield stress has great impact on the rising velocity. In the case of multiple bubbles flowing vertically, it is observed that the displacement of one bubble influences the rising velocity of the others, causing them to approach each other. As the distance between the bubbles increases the interference is reduced and the bubbles begin to flow as single ones. When two bubbles are horizontally positioned, they can approach or move away from each other, depending on the initial distance between them. Furthermore, the bubbles shape is analyzed as a function of the governing parameters. It is observed that for lower Reynolds number the bubbles present a circular shape, but as inertia increases the bubble becomes ellipsoidal.

**Keywords:** Viscoplastic fluids, Yield stress, Bubble displacement.

### 1. INTRODUCTION

Gas bubble displacement in viscoplastic fluids is present in a large number of industrial applications such as food processing, cosmetic industry, drilling and cementing of oil wells. In some applications bubbles are desired, like in the fabrication of aerated chocolate, while in others the displacement can be extremely dangerous, as during gas invasion in oil wells cementing process. Gaining a better understanding of the bubble displacement in this type of complex fluid is very important to the process analysis and optimization. This work presents a numerical analysis of the flow dynamics of gravity-driven air bubbles rise in viscoplastic fluids. The main characteristic of a viscoplastic fluid is the presence of a yield stress, below which the fluid is extremely structured, presenting a solid-like behavior. Many times, elasticity is important at this range of stress, and can play an important role on the flow pattern. A discussion of the yield stress and the role of elasticity in viscoplastic fluids is presented in Barnes (1999a), Barnes (1999b), dos Santos *et al.* (2014), Sikorski *et al.* (2009). There is a large number of studies in the literature comprising the behavior of bubbles in Newtonian fluids (Raymond

and Rosant (2000); Bozzano and Dente (2001); Smolianski *et al.* (2008); Sanada *et al.* (2008)). The numerical and experimental work of Magnaudet and Eames (2000) and the book written by Clift *et al.* (1978) approach very well the fundamental principles and governing equations of bubbles flowing in Newtonian fluids. Flow of bubbles through Newtonian and non-Newtonian fluids are also reviewed in Chhabra (2007) and Kulkarni and Joshi (2005). These works show that bubble shape and displacement are a result of the contribution of buoyancy, viscous forces, inertia and surface-tension. The presence of shear thinning, yield stress and elasticity play also an important role (Dubash and Frigaard (2004); Dubash and Frigaard (2007); Zhang *et al.* (2010); Fragedakis *et al.* (2016); Funfschilling and Li (2001); Sikorski *et al.* (2009); Lopez *et al.* (2017); Lind and Phillips (2010); Premrata *et al.* (2017); Amirnia *et al.* (2013); Smolianski *et al.* (2008); Tripathi *et al.* (2015); Tsamopoulos *et al.* (2008); Xu *et al.* (2017)). Despite all these and other relevant works, the displacement phenomena is not completely understood. Moreover, most of the results are per-formed for one single bubble. Islam *et al.* (2015) analyzed numerically the behavior of a pair of bubbles rising side by side in a

viscoplastic fluid. It could be noticed that a few attempts have been made to investigate this type of interaction. It is found on the referenced study that there is a repulsive effect between the rising pair of bubbles which increases with decreasing initial distance between the bubbles.

It is known that a gas bubble will flow in viscoplastic fluids only if the buoyant force is sufficient to overcome the opposing shear force due to the yield stress. Mougín *et al.* (2012) analyzed experimentally the shape and trajectory of air bubbles in a yield stress fluid, and observed the influence of internal stresses on bubble displacement. The authors show that the passage of a bubble through the tank disturbs the initial stress state and creates a mechanical history that changes the next trajectories.

Some authors evaluate the bubble shape along its path through the fluid, and some divergences are observed on the results obtained. In the experimental work by Sikorski *et al.* (2009), the authors analyze the effect of yield stress and bubble volume on the bubbles shape, and observe that all moving bubbles present a rounded head and a cusped tail. The bubbles shape are similar in appearance to the ones observed in other experimental works (Dubash and Frigaard (2004); Dubash and Frigaard (2007) and Mougín *et al.* (2012)). On the other side, when observing the results of the numerical studies made by Tsamopoulos *et al.* (2008) and Dimakopoulos *et al.* (2013), it is noticed that the bubbles present an ellipsoidal shape instead. Indeed, this comparison leads to questioning whether this difference is due to fluid elasticity, thixotropy or wall effects. Since the studies mentioned above could not reproduce consistent results to explain the different bubbles shape, the present study can be used to complement the theories about this issue.

The present work aims to present numerical results of the flow of air bubbles rising in yield stress fluids due to buoyancy, and to investigate the effects of some parameters in bubble shape and displacement. We investigate the rising of single and multiple bubbles inside a channel filled with a yield stress fluid. We first introduce the mathematical modelling of the problem under analysis, where the conservation and constitutive equations are detailed, together with the appropriate boundary conditions. In the numerical solution section, we present the numerical approach and the mesh tests. Finally, we show and discuss the results, and come up with some final remarks.

## 2. MODELING

The solution of the buoyancy driven flow of air bubbles rising through a yield stress fluid is performed using a bi-dimensional approach. The flow under analysis is laminar and transient, the air bubble follows the ideal gas law, the yield stress fluid is in-compressible, and the fluids are considered immiscible, so that the diffusivity  $D_{ij}$  is equal to zero.

The geometry is shown in Fig. 1.

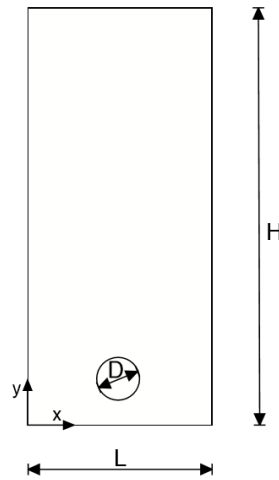


Fig. 1. The geometry.

To model the multiphase flow, we use the Volume of Fluid method (VoF) (Fluent Users Guide, 2017). The VoF solves a set of mass conservation equations to obtain the volume fraction of each phase  $j$ ,  $\alpha_j = \nabla j / \nabla$  ( $j = 1, 2, \dots, n$ ), where  $n$  is the number of phases, and  $\nabla j$  is the volume occupied by phase  $j$  in the cell control volume  $\nabla$ . The volume fraction is obtained solving  $n-1$  mass conservation equations for each phase, plus a restriction equation  $\sum_{j=1}^n \alpha_j = 1$ .

In this work only two phases are considered, namely the air and the fluid, so  $n = 2$ . When the volume fraction  $\alpha_j = 1$ , the cell contains only the phase  $j$ , and if  $\alpha_j = 0$  the cell does not contain the phase  $j$ , and if  $0 < \alpha_j < 1$  the interface between phases is positioned in the cell. The velocity and pressure are equal for both phases, and the properties are determined as the average of the properties of the phases.

Therefore, the properties  $\phi$  are obtained by:

$$\phi = \alpha_1 \phi_1 + (1 - \alpha_1) \phi_2 \quad (1)$$

The mass and momentum conservation equations are given by:

$$\frac{\partial \rho}{\partial t} + \nabla \cdot (\rho \mathbf{v}) = 0 \quad (2)$$

$$\rho \left[ \frac{\partial \mathbf{v}}{\partial t} + (\mathbf{v} \cdot \nabla) \mathbf{v} \right] = -\nabla p + \nabla \cdot \boldsymbol{\tau} + \rho \mathbf{g} \quad (3)$$

where,  $\rho$  is the mixture density,  $p$  is the pressure,  $\mathbf{g}$  is gravity, and  $\boldsymbol{\tau}$  is the deviatoric stress. The Generalized Newtonian Fluid constitutive equation is used to model the non-Newtonian fluid behavior. Therefore, the extra-stress tensor is given by:

$$\boldsymbol{\tau} = 2\eta(\dot{\gamma})\mathbf{D} \quad (4)$$

where  $\mathbf{D} \equiv 1/2 [\nabla \mathbf{v} + \nabla \mathbf{v}^T]$  is the rate-of-strain tensor, and  $(\dot{\gamma} \equiv \sqrt{2\text{tr} \mathbf{D}^2})$  is the intensity of the rate-of-strain tensor. The viscosity function is given by a regularized version of the Herschel-Bulkley model for viscoplastic fluids, given by the following equations:

$$\eta(\dot{\gamma}) = \frac{\tau_y}{\dot{\gamma}} + K (\dot{\gamma})^{n-1} \quad \text{if } \dot{\gamma} \geq \dot{\gamma}_{cr} \quad (5)$$

$$\eta(\dot{\gamma}) = \frac{\tau_y}{\dot{\gamma}_{cr}} \left[ 2 - \frac{\dot{\gamma}}{\dot{\gamma}_{cr}} \right] +$$

$$K \dot{\gamma}_{cr}^{n-1} \left[ (2-n) + (n-1) \frac{\dot{\gamma}^*}{\dot{\gamma}_{cr}} \right] \quad (6)$$

In the equations above,  $\tau_y$  is the yield stress,  $K$  is the consistency index,  $\dot{\gamma}_{cr}$  is the critical intensity of the rate-of-strain, and  $n$  is the power-law index.

The initial and boundary conditions are:

- At  $t = 0$ , the domain is filled with the viscoplastic fluid  $\alpha_1 = 1$  except at the air bubble ( $\alpha_2 = 1$ ), with diameter equal to  $D$ , which is positioned at the center of the domain at 0.01 m height from the bottom wall. The velocity is zero throughout the domain,  $\mathbf{v} = \mathbf{0}$ .
- At the top boundary, pressure is equal to the atmospheric pressure.
- At the bottom ( $y = 0$ ), left ( $x = 0$ ) and right ( $x = L$ ) walls, no slip and impermeability conditions are applied,  $\mathbf{v} = \mathbf{0}$ .

### 2.1 Dimensionless Equations

The governing equations are scaled using the following dimensionless variables:

$$x^* = \frac{x}{D} \quad y^* = \frac{y}{D} \quad v^* = \frac{v}{V_T} \quad p^* = \frac{p}{\rho g D} \quad (7)$$

$$t^* = \frac{t}{D/V_T} \quad \dot{\gamma}^* = \frac{\dot{\gamma}}{\dot{\gamma}_{cr}} \quad \eta^* = \frac{\eta}{\eta_c} \quad \rho^* = \frac{\rho}{\rho_c}$$

where  $\rho_f$  is the density of the yield stress fluid and  $V_T$  is the bubble terminal velocity. The resulting non-dimensional equations are given by:

$$\frac{\partial \alpha_j}{\partial t^*} + \mathbf{v}^* \cdot \nabla \alpha_j = 0 \quad (8)$$

$$\frac{\partial \rho^*}{\partial t^*} + \nabla \cdot (\rho^* \mathbf{v}^*) = 0 \quad (9)$$

$$\frac{\partial \mathbf{v}^*}{\partial t^*} + (\mathbf{v}^* \cdot \nabla^*) \mathbf{v}^* = -\nabla^* p^* + \frac{1}{Re} \nabla^* \cdot [Bn + (1 - Bn) \dot{\gamma}^{*n}] \quad (10)$$

$$\frac{\partial \mathbf{v}^*}{\partial t^*} + (\mathbf{v}^* \cdot \nabla^*) \mathbf{v}^* = -\nabla^* p^* + \frac{1}{Re} \nabla^* \cdot \left[ Bn \frac{\dot{\gamma}^*}{\dot{\gamma}_{cr}} \left[ 2 - \frac{\dot{\gamma}^*}{\dot{\gamma}_{cr}} \right] + (1 - Bn) \dot{\gamma}_{cr}^{(n-1)} \dot{\gamma}^* \right] \left[ (2-n) + (n-1) \frac{\dot{\gamma}^*}{\dot{\gamma}_{cr}} \right] \quad (11)$$

where Eq. (10) stands when the stress is above the yield stress, and Eq. (11) is used otherwise.

The non-dimensional governing parameters are depicted below:

$$Re \equiv \frac{\rho_f V_T D}{\eta_c} \quad Bn = \frac{\tau_y}{\eta_c \dot{\gamma}_{cr}} \quad (12)$$

where  $Re$  is the Reynolds number, and  $Bn$  is the Bingham number. The characteristic viscosity,  $\eta_c$ , is the viscosity of the yield stress fluid obtained at the characteristic rate-of-deformation, defined as  $\dot{\gamma}_c \equiv V_T/D$ .

### 3. NUMERICAL SOLUTION

The governing conservation equations of mass and momentum are solved using the finite volume method, with the Fluent® software (Ansys Inc.). To model the multiphase flow we use the Volume of Fluid (VOF) method. [Aniszewski et al. \(2014\)](#)

discuss about the applicability of VOF method to solve multiphase flows. Other methods such as Direct Numerical Simulation (DNS) ([Tryggvason et al. \(2006\)](#)), or the level set method ([Strubelj and Tiselj \(2007\)](#), [Balcazar et al. \(2014\)](#)) are also usually employed in such problems with good results. The pressure-velocity coupling equation was solved using the pressure implicit with the splitting of operators (PISO) algorithm. The geometric reconstruction approach was adopted to track the interface between the two phases using a linear approximation. The discretization schemes for the mass and momentum equation were the PRESTO and QUICK schemes, respectively, chosen accordingly the characteristics of the problem (Fluent Users Guide, 2017).

The numerical solution was modelled to simulate a common geometry found in the oil industry. Then, we consider an annular space between a 12" oil well and a 9 5/8" casing, and neglect the curvature since  $(D_o - D_i)/D_o$  is small and equal to 0.245. Therefore, the geometry analyzed is given by 2 parallel plates and the bubble is represented by a circle initially positioned in the middle of the two plates, as show in Fig. 1. A structured mesh is used, with 51209 elements (1250 divisions in the vertical direction and 42 divisions in the horizontal direction). The structured meshes used in the numerical solution were generated in ICFM CFD® software (Ansys Inc.). Mesh tests were performed for a case with a single bubble. Three different meshes were analyzed: Mesh 1 with 690 divisions at the axial direction and 70 divisions at the horizontal direction (690x70) and 47610 elements; Mesh 2, with 1250x42 divisions and 51209 elements; and Mesh 3, with 2091x70 divisions and 1444210 elements. The channel aspect ratio was held fixed:  $H/L = 30.3$ , the initial bubble diameter is equal to  $D/L = 0.12$ ,  $Re = 0.12$ , and  $Bn = 0.42$ . The results are shown in Fig. 2. It can be noted that the single bubble rising velocities obtained with Mesh 2 are very close as those obtained with Mesh 3, the error in the bubble terminal velocity is below 1%. Therefore, Mesh 2 was adopted throughout this study to take into account both the computational accuracy and the simulation time consumption. It is worth mentioning that with the mesh used, the number of cells in each bubble varies from 5 to 213. The smaller bubbles ( $D/L=0.06$  and  $0.09$ ) presented the lower number of cells, 5 and 9, respectively. Above  $D/L = 0.12$  the number of cells in each bubble is always above 20. Another important parameter in the solution is the regularization parameter for the modified Herschel Bulkley equation, namely the critical shear rate  $\dot{\gamma}_{cr}$ , defined in Eq. 6. It is well known in the literature that the regularized viscoplastic models give good results if the regularization parameter is defined so that the viscosity at very low shear rates are larger than  $1000\eta_c$  (e.g. [Burgos and Alexandrou \(1999\)](#), [Mitsoulis et al. \(2006\)](#), [Naccache and Barbosa \(2007\)](#)). To satisfy this condition, the values of  $\dot{\gamma}_{cr}/\dot{\gamma}_c$  used in the present work are always below  $10^{-3}$ . A test was performed for the case with  $\tau_y = 2$  Pa and  $D/L = 0.12$ , using a lower value of  $\dot{\gamma}_{cr}/\dot{\gamma}_c (\approx 10^{-5})$ , to verify if the results were independent of the regularization parameter. The difference between the

terminal bubble velocity was below 3%.

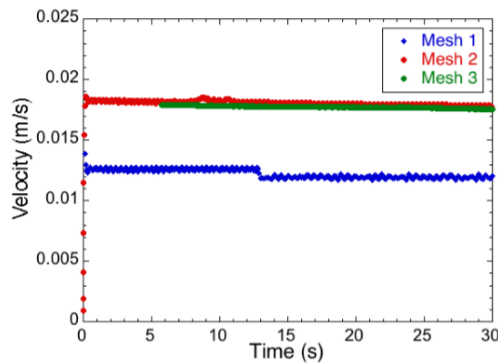


**Fig. 2. Bubble rising velocity as a function of time for meshes 1 (690x70), 2 (1250x42), and 3 (20191x70).**

#### 4. RESULTS AND DISCUSSION

The effects of bubble diameter, yield stress, and Reynolds number on the bubble displacement through the channel are evaluated for single and multiple bubbles.

##### 4.1 Single Bubble

We investigated the case of single bubbles flowing in a yield stress material modeled by the regularized Herschel-Bulkey equation (Eq. 6). The fluid density is held fixed and equal to  $1910 \text{ kg/m}^3$ , the consistency index  $K = 1 \text{ Pa}\cdot\text{s}^n$ , and the power-law index  $n = 0.7$  are also held fixed, while the yield stress  $\tau_y$  was set equal to 1, 2 and 4 Pa. The interfacial tension between the fluid and the air bubble was kept equal to  $0.07 \text{ N/m}$ . The properties used are based in the values of a cement paste used in oil wells.

The terminal velocity as a function of the bubble radius is shown in Fig. 3 for  $\tau_y = 1, 2$  and 4. As expected, smallest bubbles tend to have more difficulty to rise, so the bubble terminal velocity increases with the bubble size due to buoyancy forces. It can also be seen that below a certain critical diameter,  $D/L \approx 0.05$ , buoyancy forces can't surpass the yielding limit due to yield stress, so the bubble doesn't move. The results also shown that the velocity of the bubbles decreases with the yield stress, because the viscosity levels are higher. This effect is also addressed in Fig. 4, where it is shown the decrease of bubble terminal velocity with the increase of yield stress for  $D/L = 0.12$ . In this case, it is noted that for yield stress above around 6 Pa, buoyancy can't overcome the yield stress and the bubble remains stagnant. This can be also observed on Fig. 5, where it is noted that the Reynolds number decreases with the Bingham number up to a certain value of  $Bn$  above which the force balance between yield stress and buoyancy leads the bubble to remain stagnant. These results are in qualitative agreement with the ones obtained in [Dimakopoulos \*et al.\* \(2013\)](#) and [Lopez \*et al.\* \(2017\)](#). Fig. 3 also shows a decrease in the slope in the terminal velocity behavior, possible due to wall effects, as the bubble

dimensionless diameter is around 0.25, with this value increasing as yield stress increases. To verify if wall effects are relevant, cases were simulated with a larger distance between plates ( $L = 0.066 \text{ m}$ ), twice the original size. The comparison is shown in Fig. 6, where it can be noted that there is some wall effect when  $D/L$  increases, especially above the value of  $D/L$  close to that inflection point at the velocity curve, where the velocity decreases up to 25% due to the influence of wall.

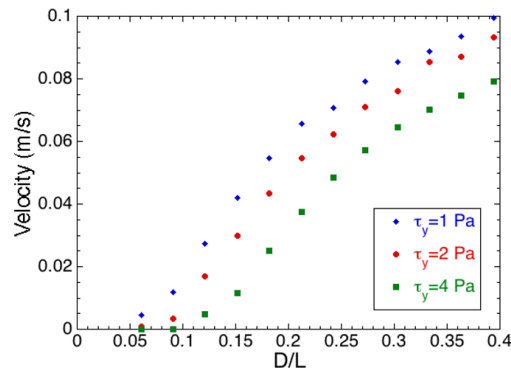


**Fig. 3. Bubble terminal velocity as a function of  $D/L$  for  $\tau_y = 1, 2$  and 4 Pa.**

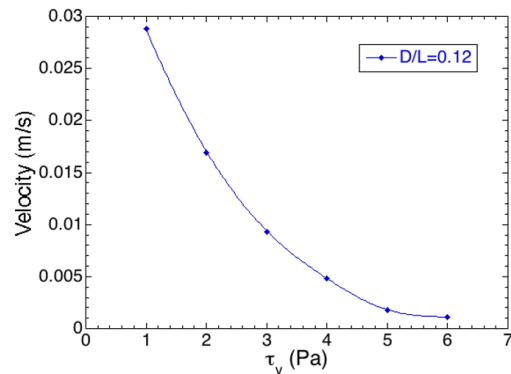


**Fig. 4. Effect of yield stress on bubble terminal velocity for  $D/L = 0.12$ .**

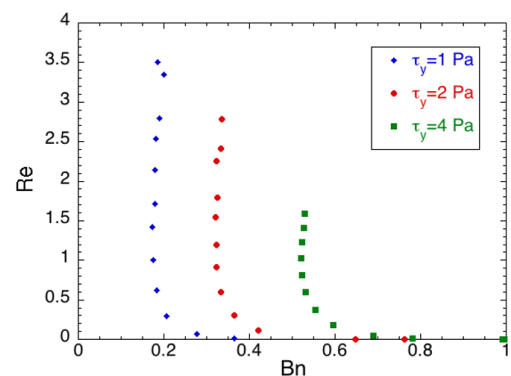


**Fig. 5. Reynolds number as a function of Bingham number.**

The wall effect can be also noted with the aid of the velocity and rate-of-deformation fields, which are shown in Figs. 7 and 8 for bubble radius equal to  $0.002$  ( $D/L = 0.12$ ),  $0.003$  ( $D/L = 0.18$ ) and  $0.004$

( $D/L = 0.24$ ) m and  $\tau_y = 2$  Pa. It can be observed that the wall has no effect on the fields for the bubble with  $D/L = 0.12$ , but as the bubble radius increases the effect is significant both in the velocity and strain rate fields, since for both fields the region affected by the presence of the bubble reaches the walls.

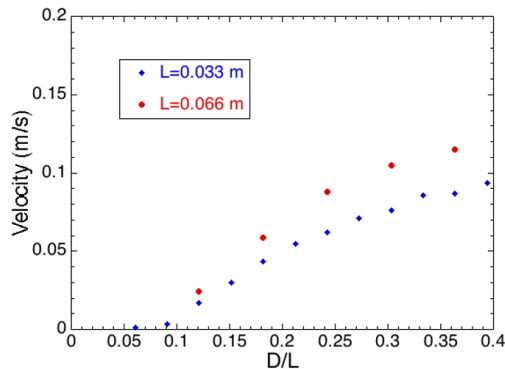


**Fig. 6. Wall effect on bubble velocity for  $\tau_y = 2$  Pa.**

Fig. 9 shows the bubble shape as a function of the Reynolds number, which is calculated using the terminal velocity obtained numerically. As it can be seen, the bubble has a spherical shape at lower Reynolds numbers, when inertia is negligible, and as it increases the bubble acquires an ellipsoidal shape due to inertia effects. When the bubble is sufficiently small the surface tension forces tend to maintain the spherical shape. As the bubble grows, inertia forces grow and exceed the surface tension, which becomes negligible. These results are in contrast with the ones observed in the experimental study made by Sikorski *et al.* (2009) and Lopez *et al.* (2017), where it was observed bubble shapes with a rounded head and a cusped tail. However, this difference can be due to elasticity that is present in the fluid used in the experiments. In this work, we don't consider elasticity in fluid behavior. Indeed, the bubble shapes found in this work are in agreement with the experimental ones found in Lopez *et al.* (2017) for the less concentrated Carbopol dispersions, which have almost no elasticity. On the other hand, the shapes are very different from the experimental bubble shapes obtained for higher concentrated dispersions, which present a stronger elastic behavior below yield stress. It is also worth comparing the bubble shapes with the ones shown in the  $Re \times Eo$  map for Newtonian fluids (Grace (1973)), where  $Eo = \rho g D^2 / \sigma$  is the Etvos number and  $\sigma$  is the interfacial tension. In the results shown in Fig. 9,  $Eo$  varies from 1 ( $Re = 0.007$ ) to 45 ( $Re = 2.41$ ), where the bubble shape goes from spherical to ellipsoidal and ellipsoidal cap for that range of Reynolds number.

As discussed in Lopez *et al.* (2017), the critical  $Bn$  above which the bubble remains stagnant is difficult to be determined, either due to numerical or experimental difficulties related to the size of mesh and model approximations and experimental limitations. In this work, we couldn't obtain the

value of the critical Bingham, but we estimated it being around 0.80. This result was compared to the ones obtained in the experimental work of Sikorski *et al.* (2009). Similar to the Bingham number, they defined a yield number  $Y = 2\pi\tau_y W^2 / \rho g V$ , where  $W$  is the bubble width and  $V$  is the bubble volume. The critical yield number obtained in Sikorski *et al.* (2009) was equal to 0.5, while in the present work the estimated value for the critical yield number is around 1. It is also worth mentioned the theoretical value obtained in Dubash and Frigaard (2004), equal to 0.87.

## 4.2 Multiple Bubbles Arranged Vertically

We now present the results for multiple vertical in-line bubbles rising through a yield stress fluid. Figs. 10–16 show the bubbles Reynolds numbers as they move up between the plates, for  $D/L$  equal to 0.12, 2 and 3 bubbles, yield stress equal to 2 and 4 Pa, and different initial distances  $d_b$  between bubbles ( $d_b/L = 0.3, 0.6, 0.9$  and 1.2).

Figure 10 shows the results for the displacement of one bubble ( $D=L = 0:12$ ) through the fluid with  $\tau_y = 2$  Pa, where it can be observed that the Reynolds number is almost constant ( $\approx 0:06$ ) throughout the channel. Figs 11 – 14 show the flow of two bubbles of the same radius ( $D=L = 0:12$ ), with a space between them of  $d_b=L = 0:3; 0:6; 0:9$  and 1.2 respectively, in a fluid with yield stress equal to 2 Pa.

Analyzing these plots it can be observed that the second bubble rises with a larger Reynolds number (or velocity) than the first bubble, because the first bubble shear the fluid decreasing its viscosity. Then, the second bubble flows through a less viscous fluid, reaching larger velocities. At a certain point the bubbles collapse and a velocity peak is observed. Later on, the velocity decreases to a value mildly higher than that of the original bubbles, since the new bubble is bigger, which leads to higher buoyancy forces. This behavior is observed for the cases where the distance between bubbles is equal to  $d_b/L = 0.3, 0.6$  and 0.9. It can also be observed that as the bubble spacing increases, the velocity peak is lower and occurs later. Moreover, the results obtained for  $d_b/L = 1.2$ , shown in Fig. 14, show that as the distance between bubbles in-creases, the first bubble no longer affect the flow of the second bubble and vice-versa. It can be noticed that the bubbles flow with the same velocity, equal to the single bubble case, and don't collapse anymore. This happens because the fluid structure breakage region below the first bubble is limited and doesn't reach the second bubble.

Fig. 15 shows the Reynolds number for the flow of two bubbles with  $D/L = 0.12$  and distance between them equal to  $d_b/L = 0.6$ , through the fluid with yield stress equal to 4 Pa. It can be observed that despite the fact that the velocity peak is lower than the one obtained for the case with the lower yield stress, as expected since in this case the fluid is more viscous, the position where the bubbles collapse remains the same.

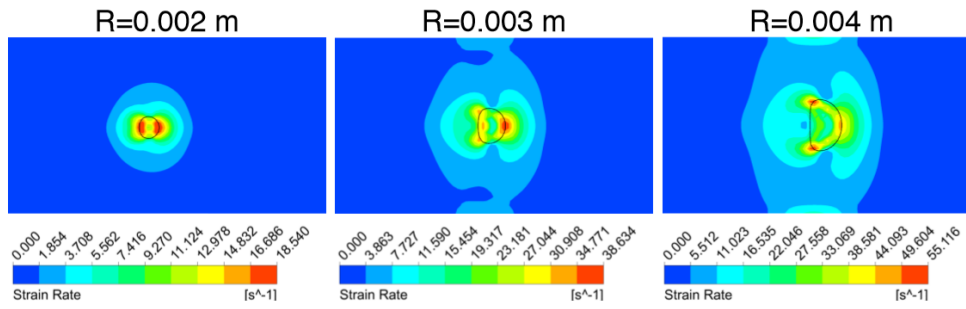


Fig. 7. Rate-of-deformation field for  $\tau_y = 2$  Pa and  $D/L = 0.12, 0.18,$  and  $0.24$ .

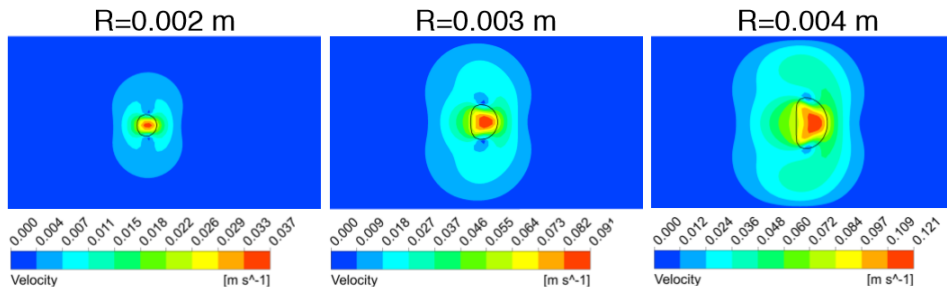


Fig. 8. Velocity magnitude field for  $\tau_y = 2$  Pa and  $D/L = 0.12, 0.18,$  and  $0.24$ .

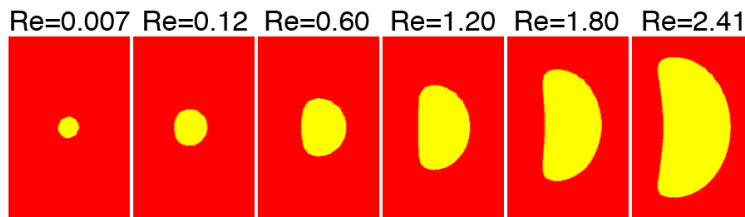


Fig. 9. Bubble shape as a function of Reynolds number for  $\tau_y = 2$  Pa and  $D/L = 0.12$ .

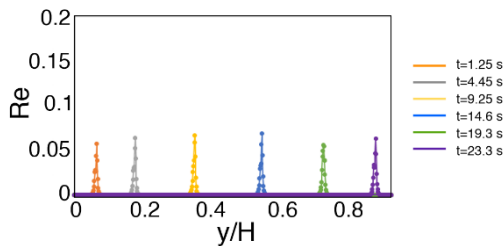


Fig. 10. Reynolds number versus vertical position for 1 bubble displacement at different times,  $D/L = 0.12$  and  $\tau_y = 2$  Pa.

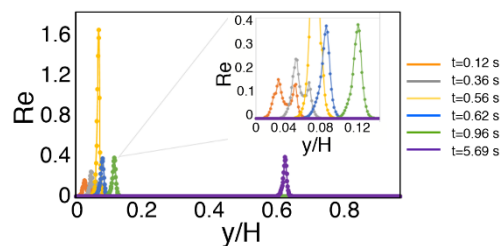


Fig. 11. Reynolds number versus vertical position for 2 bubbles displacement at different times,  $D/L = 0.12$ ,  $\tau_y = 2$  Pa, and distance between bubbles equal to  $d_b/L = 0.3$ .

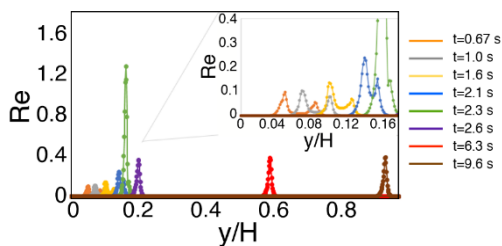


Fig. 12. Reynolds number versus vertical position for 2 bubbles displacement at different times,  $D/L = 0.12$ ,  $\tau_y = 2$  Pa, and distance between bubbles equal to  $d_b/L = 0.6$ .

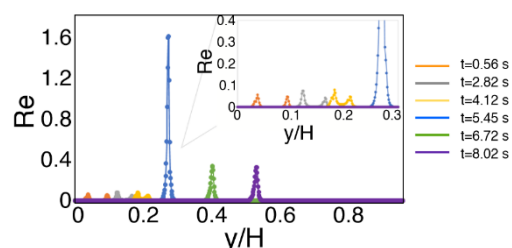
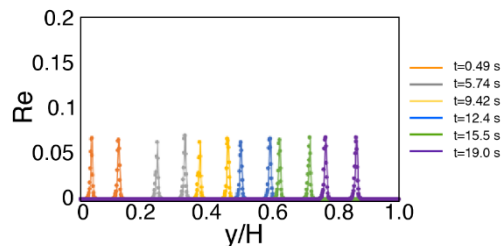
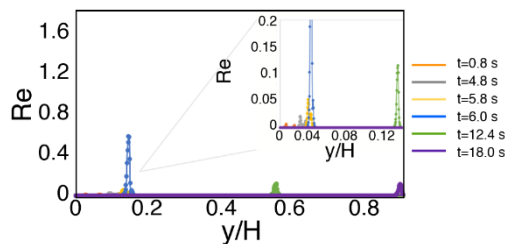


Fig. 13. Reynolds number versus vertical position for 2 bubbles displacement at different times,  $D/L = 0.12$ ,  $\tau_y = 2$  Pa, and distance between bubbles equal to  $d_b/L = 0.9$ .

The displacement of three bubbles is show in Fig. 16, for  $d_b/L = 0.3$ . It is noted that the first bubble has a velocity much lower than the next ones. Then, the second bubble reaches the first one and collapse with it. After that, this new bubble flows with a higher velocity, moving apart from the third one. Therefore, just after the collapse of the two first bubbles, the velocity of the second bubble is slightly lower, but as they move apart the fluid between then build-up and its viscosity increases, which leads to a decrease of the velocity of the second bubble. It can be noted that from  $t_5 = 1$  s to  $t_6 = 4.3$  s the velocity of the two bubbles remains almost the same, indicating that close to this point they are already in a distance where the second bubble is not affected by the first one.



**Fig. 14. Reynolds number versus vertical position for 2 bubbles displacement at different times,  $D/L = 0.12$ ,  $\tau_y = 2$  Pa, and distance between bubbles equal to  $d_h/L = 1.2$ .**



**Fig. 15. Reynolds number versus vertical position for 2 bubbles displacement at different times,  $D/L = 0.12$ ,  $\tau_y = 4$  Pa, and distance between bubbles equal to  $d_h/L = 0.6$ .**

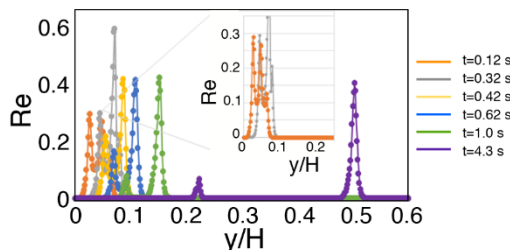


**Fig. 16. Reynolds number versus vertical position for 3 bubbles displacement at different times, bubbles radius equal to 2 mm,  $\tau_y = 2$  Pa, and distance between bubbles equal to  $d_h/L = 0.3$ .**

The velocity and strain rate fields for two and three bubbles displacement are shown in Figs. 18 – 20. Fig. 18 shows the velocity and strain rate fields for

the displacement of two bubbles with dimensionless diameter  $D/L = 0.12$  and  $d_b/L = 0.9$ . The fluid has the yield stress equal to  $\tau_y = 2$  Pa. It can be seen that at the beginning ( $t = 1$  s) the fields dont interfere much on each other. As the bubbles rise, they get closer because the velocity of the second bubble increases. It clear that the velocity and strain rate fields ahead the second bubble are higher than ahead the first one. This is caused by the flow of the first bubble, which shear the fluid as it passes through, breaking the fluid structure and lowering the viscosity and the drag force around the second bubble. It is also important to mention that there is a small difference between the bubbles shape due to the approximation that is made when the spherical bubbles are generated. Since the mesh elements are rectangular, the initial bubble shapes are not exactly the same causing a small difference in the velocity and strain rate fields around them. To mitigate this problem it would be necessary to refine the mesh even more but since the differences are very mild, and don't affect significantly the terminal velocities, the computational cost increase would not worth it. The velocity and strain rate fields for the displacement of three bubbles with  $D/L = 0.12$ , and  $d_b/L = 0.9$  are shown in Figs. 19 and 20, for the fluid with the yield stress equal to  $\tau_y = 2$  Pa. Higher velocities and strain rates occur around the second and third bubbles, the last one moves faster until it collapses with the second bubble. After that, the new collapsed bubble flows with higher velocity due to its larger size, and moves toward the first one. It is interesting to note that this behavior is different from the one analyzed in Fig. 16, where  $d_b/L$  is lower, and the second bubble reached the first one before. The comparison of these two results show that the distance between the bubbles plays an important role on the bubbles flow.

### 4.3 Pair of bubbles Arranged Horizontally

Three simulations were carried out considering two bubbles rising side by side. Fig. 21 shows the effect of the horizontal distance between the bubbles on their displacement. In each case the two bubbles have the diameter equal to 2 mm ( $D/L = 0.12$ ), and the fluid has the yield stress equal to  $\tau_y = 2$  Pa. The dimensionless distance between bubbles is equal to  $d_h/L = 0.09, 0.21, 0.33$ .

According to Fig. 21, it can be noticed that when the bubbles are positioned closest to each other (lowest  $d_h/L$ ) they move away from each other until a certain distance, from where its distance is kept constant. It is believed that this behavior is due to a strong repulsion effect resulting from the large amount of vortices generated between the bubbles. These results are in agreement with the numerical study by [Islam \*et al.\* \(2015\)](#). On the other hand, for the largest distance between bubbles ( $d_h/L = 0.33$ , Fig. 21c), the opposite trend is observed. In this case, the bubbles come closer to each other until a certain distance where they keep the same distance as the other cases. It is believed that for this bubbles interval, the repulsive force is not present anymore and the strain rate field generates velocities toward the channel center, making the bubbles get closer to each other. It is suspected that this behavior could be due to wall

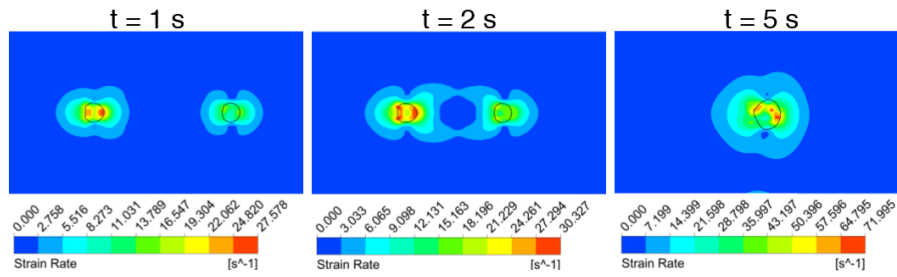


Fig. 17. Rate-of-deformation field for 2 bubbles displacement at different times,  $D/L = 0.12$ ,  $\tau_y = 2$  Pa, and  $d_h/L = 0.9$ .

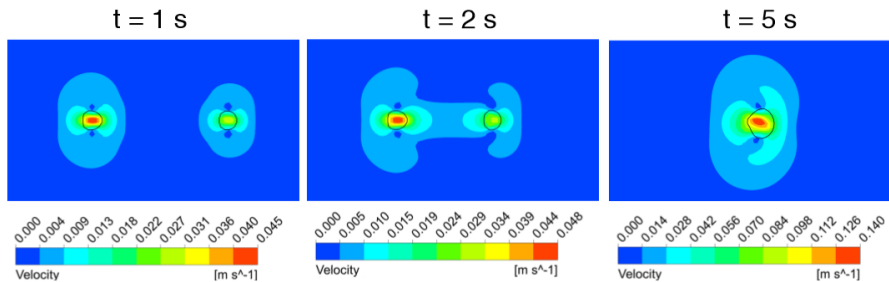


Fig. 18. Velocity magnitude field for 2 bubbles displacement at different times,  $D/L = 0.12$ ,  $\tau_y = 2$  Pa, and  $d_h/L = 0.9$ .

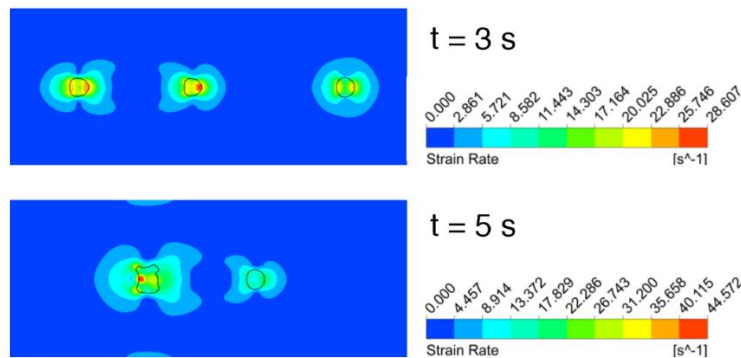


Fig. 19. Rate-of-deformation field for 3 bubbles displacement at different times,  $D/L = 0.12$ ,  $\tau_y = 2$  Pa, and  $d_h/L = 0.9$ .

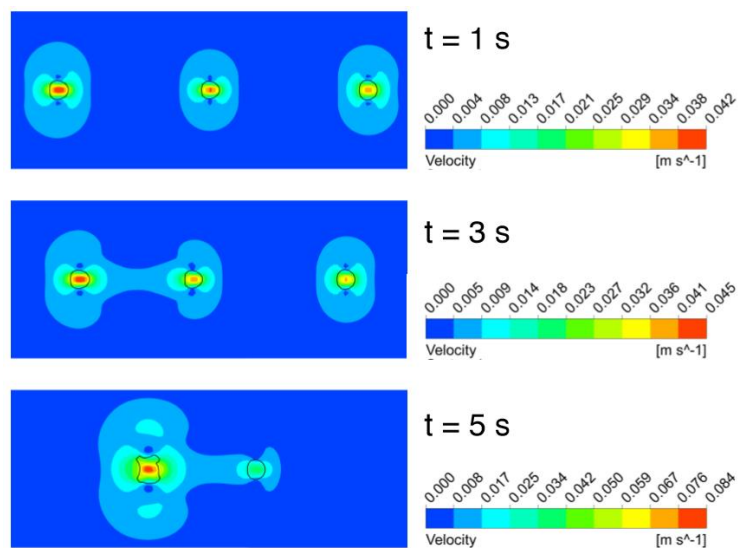
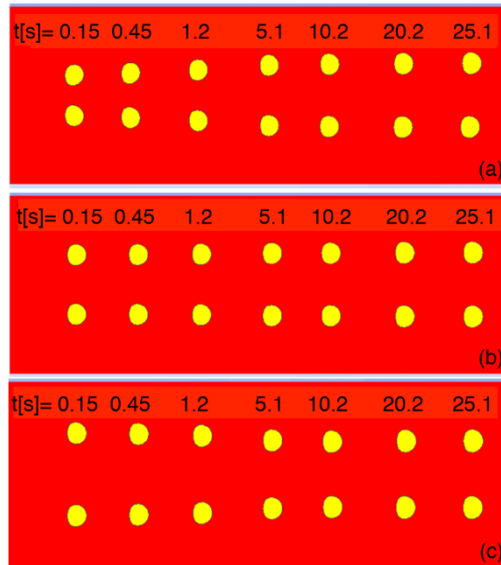


Fig. 20. Velocity magnitude field for 3 bubbles displacement at different times,  $D/L = 0.12$ ,  $\tau_y = 2$  Pa, and  $d_h/L = 0.9$ .

effects, but a simulation was carried out for a channel width ( $L$ ) twice larger than the one show in these cases, but no difference in the bubbles velocity was observed.



**Fig. 21. Two horizontal bubbles displacement,  $D/L = 0.12$ ,  $\tau_y = 2$  Pa, and horizontal distance between bubbles equal to: (a)  $d_h/L = 0.09$ ; (b)  $d_h/L = 0.21$ ; (c)  $d_h/L = 0.33$ .**

## 5. FINAL REMARKS

This work presents a numerical study of the flow of air bubbles through yield stress fluids. This problem is found in several industrial processes, e.g. gas invasion in oil wells during cementation operations. Therefore, it is of interest to predict the flow dynamics and the bubble shape. The volume of fluid method (VoF) is employed to deal with the multiphase flow gas/fluid, whereas the Finite Volume method is used to solve the governing conservation equations. All the numerical simulations are per-formed with the Fluent software<sup>®</sup>.

First, we analyze the shape and velocity of a single bubble as a function of bubble diameter and fluid yield stress. The results show that as the bubble grows, the rising velocity increases and the bubble shape changes from a spherical to an ellipsoidal shape due to inertia effects. It was also observed that the rising velocity is reduced as the fluids yield stress increases. Wall effects were also observed and it was found that it influences the rising velocity when the ratio  $D/L$  (where  $L$  is the distance between the plates) is higher than around 0.25, where the velocity and strain rate field begins to be influenced by the wall. It was also noted that very small bubbles are not able to rise because buoyancy forces can't overcome the yield stress.

Considering the vertical multiple in line bubbles flow, it could be verified that the distance between the bubbles will interfere on the rising behavior. At

the present study, only after a bubbles interval ratio equal to  $db/L = 1.2$  this interference is not significant and the bubbles move separately. Moreover, considering the numerical solution of the cases carried out for a pair of bubbles rising side by side it was possible to observe that there is a repulsive effect between the bubbles that increases as this interval decreases.

## ACKNOWLEDGMENTS

This study was financed in part by the Coordenação de Aperfeiçoamento de Pessoal de Nível Superior-Brasil (CAPES) - Finance Code 001. The authors also acknowledge PUC-Rio, Petrobras, FAPERJ and CNPq for financial support.

## REFERENCES

- Amirnia, S., J. R. de Bruyn, M. A. Bergougnou, and A. Margaritis (2013). Continuous rise velocity of air bubbles in non-newtonian biopolymer solutions. *Chemical Engineering Science* 94, 60–68.
- Aniszewski, W., T. Menard, and M. Marek (2014). Volume of fluid (vof) type advection methods in two-phase flow: A comparative study. *Computers and Fluids* 97, 52–73.
- Balcazar, N., L. Jofre, O. Lehmkuhl, J. Rigola, J. Castro, and A. Oliva (2014). A finite-volume/level-set interface capturing method for unstructured grids: simulations of bubbles rising through viscous liquids. *WIT Transactions on Engineering Science* 82, 239–250.
- Barnes, H. A. (1999a). A brief history of the yield stress. *Applied Rheology* 9, 262–266.
- Barnes, H. A. (1999b). The yield stress—a review. *Journal of Non-Newtonian Fluid Mechanics* 81, 133–178.
- Bozzano, G. and M. Dente (2001). Shape and terminal velocity of single bubble motion: a novel approach. *Computers and Chemical Engineering* 25, 571–576.
- Burgos, G. R. and A. N. Alexandrou (1999). Flow development of Herschel-Bulkley fluids in a sudden 3-D expansion. *Journal of Rheology* 43(3), 463–483.
- Chhabra, R. P. (2007). *Bubbles, Drops, and Particles in Non-Newtonian Fluids* (2 ed.). Taylor & Francis.
- Clift, R., J. R. Grace, and M. E. Weber (1978). *Bubbles, Drops, and Particles*. New York: Academic Press.
- Dimakopoulos, Y., M. Pavlidis, and J. Tsamopoulos (2013). Steady bubble rise in Herschel-Bulkley fluids and comparison of predictions via the augmented Lagrangian method with those via the Papanastasiou model. *Journal of Non-Newtonian Fluid Mechanics* 200, 34–51.
- dos Santos, D. D., S. L. Frey, M. F. Naccache, and P.

- R. de Souza Mendes (2014). Flow of elasto-viscoplastic liquids through a planar expansion-contraction. *Rheologica Acta* 53, 31–41.
- Dubash, N. and I. Frigaard (2004). Conditions for static bubbles in viscoplastic fluids. *Physics Fluids* 16, 4319–4330.
- Dubash, N. and I. Frigaard (2007). Propagation and stopping of air bubbles in carbopol solutions. *Journal of Non-Newtonian Fluid Mechanics* 142, 123–134.
- Fraggedakis, D., Y. Dimakopoulos, and J. Tsamopoulos (2016). Yielding the yield-stress analysis: a study focused on the effects of elasticity on the settling of a single spherical particle in simple yield-stress fluids. *Soft Matter* 12, 5378–5401.
- Funfschilling, D. and H. Z. Li (2001). Flow of non-newtonian fluids around bubbles: Piv measurements and birefringence visualisation. *Chemical Engineering Science* 56, 1137–1141.
- Grace, J. R. (1973). Shapes and velocities of bubbles rising in infinite liquids. *Transactions of the Institution of Chemical Engineers* 51, 116–120.
- Islam, M. T., P. Ganesan, and J. Cheng (2015). A pair of bubbles' rising dynamics in a xanthan gum solution: a cfd study. *The Royal Society of Chemistry* 5, 7819–7831.
- Kulkarni, A. and J. B. Joshi (2005). Bubble formation and bubble rise velocity in gas-liquid systems: A review. *Industrial & Engineering Chemistry Research* 44, 5873–5931.
- Lind, S. J. and T. N. Phillips (2010). The effect of viscoelasticity on a rising gas bubble. *Journal of Non-Newtonian Fluid Mechanics* 165, 852–865.
- Lopez, W. F., M. F. Naccache, and P. R. de Souza Mendes (2017). Rising bubbles in yield stress materials. *Journal of Rheology* 62(1), 209–219.
- Magnaudet, J. and I. Eames (2000). The motion of high-Reynolds-number bubbles in inhomogeneous flows. *Annual Review of Fluid Mechanics* 32, 659–708.
- Mitsoulis, E., S. Marangoudakis, M. S. and Th. Zisis, and N. A. Malamaris (2006). Pressure-driven flows of bingham plastics over a square cavity. *Journal of Fluids Engineering* 128, 993–1003.
- Mougin, N., A. Magnin, and J. M. Piau (2012). The significant influence of internal stresses on the dynamics of bubbles in a yield stress fluid. *Journal of Non-Newtonian Fluid Mechanics* 171-172, 42–55.
- Naccache, M. F. and R. S. Barbosa (2007). Creeping flow of viscoplastic materials through a planar expansion followed by a contraction. *Mechanics Research Communications* 34, 423–431.
- Premlata, A. R., M. K. Tripathi, B. Karri, and K. C. Sahu (2017). Dynamics of an air bubble rising in a non-newtonian liquid in the axisymmetric regime. *Journal of Non-Newtonian Fluid Mechanics* 239, 53–61.
- Raymond, F. and J. Rosant (2000). A numerical and experimental study of the terminal velocity and shape of bubbles in viscous liquids. *Chemical Engineering Science* 55, 943–955.
- Sanada, T., K. Sugihara, M. Shirota, and M. Watanabe (2008). Motion and drag of a single bubble in super-purified water. *Fluid Dynamics Research* 40, 534–545.
- Sikorski, D., H. Tabuteau, and J. R. de Bruyn (2009). Motion and shape of bubbles rising through a yield-stress fluid. *Journal of Non-Newtonian Fluid Mechanics* 159, 10–16.
- Smolianski, A., H. Haario, and P. Luukka (2008). Numerical study of dynamics of single bubbles and bubble swarms. *Applied Mathematical Modelling* 32, 641–659.
- Strubelj, L. and I. Tiselj (2007). Simulation of rising bubble with conservative level set method. In *ASME (Ed.), Proceedings of FEDSM2007*.
- Tripathi, M. K., K. C. Sahu, G. Karapetsas, and O. K. Matar (2015). Bubble rise dynamics in a viscoplastic material. *Journal of Non-Newtonian Fluid Mechanics* 222, 217–226.
- Tryggvason, G., A. Esmaeeli, J. Lu, and S. Biswas (2006). Direct numerical simulations of gas/liquid multiphase flows. *Fluid Dynamics Research* 38, 660–681.
- Tsamopoulos, J., Y. Dimakopoulos, N. Chatzidai, G. Karapetsas, and M. Pavlidis (2008). Steady bubble rise and deformation in newtonian and viscoplastic fluids and conditions for bubble entrapment. *Journal of Fluid Mechanics* 601, 123–164.
- Xu, X., J. Zhang, F. Liu, X. Wang, W. Wei, and Z. Liu (2017). Rising behavior of single bubble in infinite stagnant non-newtonian liquids. *International Journal of Multiphase Flow* 95, 84–90.
- Zhang, L., C. Yang, and Z. S. Mao (2010). Numerical simulation of a bubble rising in shear-thinning fluids. *Journal of Non-Newtonian Fluid Mechanics* 165, 555–567.